

Antiferromagnetism in semiconducting $\text{KFe}_{0.85}\text{Ag}_{1.15}\text{Te}_2$ single crystals

Hechang Lei, Emil S. Bozin, Kefeng Wang, and C. Petrovic
*Condensed Matter Physics and Materials Science Department,
Brookhaven National Laboratory, Upton, NY 11973, USA*
(Dated: October 25, 2018)

We have synthesized single crystals of $\text{K}_{1.00(3)}\text{Fe}_{0.85(2)}\text{Ag}_{1.15(2)}\text{Te}_{2.0(1)}$. The materials crystallizes in the ThCr_2Si_2 structure with $I4/mmm$ symmetry and without K and Fe/Ag deficiencies, unlike in $\text{K}_x\text{Fe}_{2-y}\text{Se}_2$ and $\text{K}_x\text{Fe}_{2-y}\text{S}_2$. Transport, magnetic, and heat capacity measurements indicate that $\text{KFe}_{0.85}\text{Ag}_{1.15}\text{Te}_2$ is a semiconductor with long-range antiferromagnetic transition at $T_N = 35$ K.

PACS numbers: 74.70.Xa, 74.10.+v, 75.50.Ee, 81.05.Zx

The discovery of superconductivity in $\text{LaFeAsO}_{1-x}\text{F}_x$ ¹ has stimulated substantial interest in iron based high temperature superconductors (Fe-HTS). Until now, several Fe-HTS were discovered. They can be divided into two classes. The first class are iron pnictide materials.¹⁻³ They contain two dimensional FePn (Pn = pnictogens) tetrahedron layers and atomic sheets (e.g. Ba, K) or complex blocks (e.g. La-O(F)) along the c axis. Another class are binary iron chalcogenides FeCh (Ch = chalcogens, FeCh-11 type).⁴⁻⁶ In contrast to the diversity of iron pnictide superconductors, FeCh-11 type materials do not have any atomic or complex layers between puckered FeCh sheets.

Very recently, the discovery of $\text{A}_x\text{Fe}_{2-y}\text{Se}_2$ ($\text{A} = \text{K}, \text{Rb}, \text{Cs}$ and Tl , FeCh-122 type) with $T_c \approx 30$ K raised T_c in Fe-HTS by introducing alkali metal atomic layers between FeCh sheets.⁷⁻¹⁰ Further studies indicate that in the new superconductors the T_c gets enhanced when compared to FeCh-11 materials, but there is also a set of distinctive physical properties. FeCh-122 materials are close to the metal-semiconducting crossover and antiferromagnetic (AFM) order.⁷⁻¹⁰ This is in contrast to other superconductors which are in close proximity to the spin density wave state.¹¹ Fermi surface in FeCh-122 type Fe-HTS contains only electron like sheets without nesting features found in most other Fe-HTS.¹²

On the other hand, superconductivity in FeCh-11 materials is quite robust with respect to anion change as seen on the example of $\text{FeSe}_{1-x}\text{Te}_x$, $\text{FeTe}_{1-x}\text{Se}_x$ and $\text{FeTe}_{1-x}\text{S}_x$.⁴⁻⁶ However, in FeCh-122 compounds, superconductivity is only observed in $\text{A}_x\text{Fe}_{2-y}\text{Se}_2$ or $\text{A}_x\text{Fe}_{2-y}\text{Se}_{2-z}\text{S}_z$,¹³ while pure $\text{K}_x\text{Fe}_{2-y}\text{S}_2$ is a semiconductor with spin glass transition at low temperature.¹⁴ Moreover, the theoretical calculation indicates that the hypothetical KFe_2Te_2 , if synthesized, would have higher T_c than $\text{K}_x\text{Fe}_{2-y}\text{Se}_2$.¹⁵ Therefore, synthesis and examination of physical properties of FeCh-122 materials containing FeTe layers could be very instructive.

In this work, we report discovery of $\text{K}_{1.00(3)}\text{Fe}_{0.85(2)}\text{Ag}_{1.15(2)}\text{Te}_{2.0(1)}$ single crystals. The resistivity and magnetic measurements indicate that this compound has the semiconducting long range antiferromagnetic (AFM) order at low temperature with no superconductivity down to 1.9 K.

Single crystals of $\text{K}(\text{Fe},\text{Ag})_2\text{Te}_2$ were grown by self-

flux method reported elsewhere in detail^{14,16} with nominal composition $\text{K}:\text{Fe}:\text{Ag}:\text{Te} = 1:1:1:2$. Single crystals with typical size $5 \times 5 \times 2$ mm³ can be grown. Powder X-ray diffraction (XRD) data were collected at 300 K using 0.3184 Å wavelength radiation (38.94 keV) at X7B beamline of the National Synchrotron Light Source. The average stoichiometry was determined by examination of multiple points using an energy-dispersive x-ray spectroscopy (EDX) in a JEOL JSM-6500 scanning electron microscope. Electrical transport measurements were performed using a four-probe configuration on rectangular shaped polished single crystals with current flowing in the ab -plane of tetragonal structure. Thin Pt wires were attached to electrical contacts made of silver paste. Electrical transport, heat capacity, and magnetization measurements were carried out in Quantum Design PPMS-9 and MPMS-XL5.

Figure 1(a) shows powder XRD result and structural refinements of $\text{K}(\text{Fe},\text{Ag})_2\text{Te}_2$ using General Structure Analysis System (GSAS).^{17,18} It can be seen that all reflections can be indexed in the $I4/mmm$ space group. The refined structure parameters are listed in Table 1. The determined lattice parameters are $a = 4.3707(9)$ Å and $c = 14.9540(8)$ Å, which are reasonably smaller than those of $\text{CsFe}_x\text{Ag}_{2-x}\text{Te}_2$ ($a = 4.5058(4)$ Å and $c = 15.4587(8)$ Å),¹⁹ but much larger than those of $\text{K}_x\text{Fe}_{2-y}\text{Se}_2$ and $\text{K}_x\text{Fe}_{2-y}\text{S}_2$,^{7,14} due to smaller ionic size of K^+ than Cs^+ and larger size of Ag^+ and Te^{2-} than Fe^{2+} and Se^{2-} (S^{2-}). On the other hand, larger a -axis lattice parameter indicates that the Fe plane is stretched in $\text{K}(\text{Fe},\text{Ag})_2\text{Te}_2$ when compared to FeTe .²⁰ The crystal structure of $\text{K}(\text{Fe},\text{Ag})_2\text{Te}_2$ is shown in Fig. 1(b), where antifluorite-type Fe/Ag-Te layers and K cation layers are stacked alternatively along the c axis. XRD pattern of a single crystal (Fig. 1(c)) reveals that the crystal surface is normal to the c axis with the plate-shaped surface parallel to the ab -plane. Fig. 1(d) presents the EDX spectrum of a single crystal, which confirms the presence of the K, Fe, Ag, and Te. The average atomic ratios determined from EDX are $\text{K}:\text{Fe}:\text{Ag}:\text{Te} = 1.00(3):0.85(2):1.15(2):2.0(1)$. The value of $\text{Fe}/(\text{Ag}+\text{Fe})$ determined from XRD fitting (0.38) is close to that obtained from EDX (0.43). It suggests that Te compound prefers to contain more Ag. This might explain why pure KFe_2Te_2 can not form since large Ag^+ ions have to be

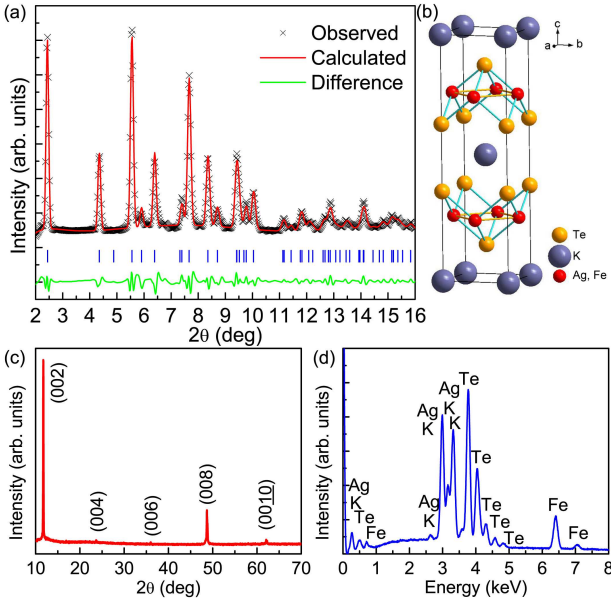


FIG. 1. (a) Powder XRD patterns of $\text{KFe}_{0.85}\text{Ag}_{1.15}\text{Te}_2$. (b) Crystal structure of $\text{KFe}_{0.85}\text{Ag}_{1.15}\text{Te}_2$. The big blue, small red and medium orange balls represent K, Fe/Ag, and Te ions. (c) Single crystal XRD of $\text{KFe}_{0.85}\text{Ag}_{1.15}\text{Te}_2$. (d) The EDX spectrum of a single crystal.

TABLE I. Structural parameters for $\text{K}(\text{Fe},\text{Ag})_2\text{Te}_2$ at room temperature. Values in brackets give the number of equivalent distances or angles of each type. The occupancies of K and Te are fixed during fitting.

Chemical Formula	$\text{K}_{1.00(3)}\text{Fe}_{0.85(2)}\text{Ag}_{1.15(2)}\text{Te}_{2.0(1)}$				
Space Group	I4/mmm				
a (Å)	4.3707(9)				
c (Å)	14.9540(8)				
V (Å ³)	285.7(1)				
Interatomic Distances (Å)		Bond Angles (°)			
$d_{\text{Fe/Ag}-\text{Fe/Ag}}$ [4]	3.0906(4)	Te-Fe/Ag-Te [2]	104.44(3)		
$d_{\text{Fe/Ag}-\text{Te/Ag}}$ [4]	2.7651(5)	Te-Fe/Ag-Te [4]	112.05(4)		
Anion Heights (Å)		1.694(7)			
Atom	x	y	z	Occ	U_{iso} (Å ²)
K	0	0	0	1.00	0.056(5)
Fe	0.5	0	0.25	0.76(8)	0.035(7)
Ag	0.5	0	0.25	1.24(8)	0.035(7)
Te	0.5	0.5	0.1367(5)	1.00	0.034(4)

introduced in order to match the rather large Te^{2-} anions and keep the stability of the structure. On the other hand, it should be noted that there are no K or Fe/Ag deficiencies in $\text{K}(\text{Fe},\text{Ag})_2\text{Te}_2$. This is rather different from $\text{K}_x\text{Fe}_{2-y}\text{Se}_2$ and $\text{K}_x\text{Fe}_{2-y}\text{S}_2$.^{7,14} Moreover, synchrotron powder X-ray refinement and EDX were consistent with either stoichiometric Te or not more than 5% vacancies (i.e., $\text{Te}_{1.9}$)

Figure 2 shows the temperature dependence of the in-plane resistivity $\rho_{ab}(T)$ of the $\text{KFe}_{0.85}\text{Ag}_{1.15}\text{Te}_2$ sin-

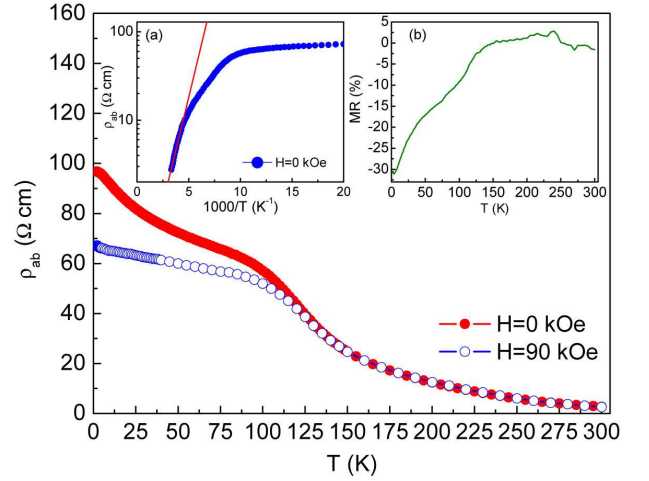


FIG. 2. Temperature dependence of the in-plane resistivity $\rho_{ab}(T)$ of the $\text{KFe}_{0.85}\text{Ag}_{1.15}\text{Te}_2$ single crystal with $H = 0$ (closed red circle) and 90 kOe (open blue square, $H \parallel c$). Inset (a) shows the fitted result using thermal activation model for $\rho_{ab}(T)$ at zero field where the red line is the fitting curve. Inset (b) exhibits the temperature dependence of MR(T) for $\text{KFe}_{0.85}\text{Ag}_{1.15}\text{Te}_2$.

gle crystal for $H = 0$ and 90 kOe. The resistivity increases with decreasing the temperature with a "shoulder" appearing around 100 K. The room-temperature value ρ_{ab} is about 2.7 $\Omega\text{-cm}$, which is much larger than in superconducting $\text{K}_x\text{Fe}_{2-y}\text{Se}_2$ and semiconducting $\text{K}_x\text{Fe}_{2-y}\text{S}_2$.^{14,16} The semiconducting behavior might be related to the random distribution of Fe and Ag ions in the Fe/Ag plane which induces a random scattering potential, similar to the effect of Fe deficiency in the FeSe or FeS plane.^{14,21} By fitting the $\rho_{ab}(T)$ at high temperature using the thermal activation model $\rho = \rho_0 \exp(E_a/k_B T)$, where ρ_0 is a prefactor and k_B is Boltzmann's constant (inset (a) of Fig. 2), we obtained $\rho_0 = 71(6)$ m $\Omega\text{-cm}$ and the activation energy $E_a = 96(2)$ meV in the temperature range above 200 K, which is larger than that of $\text{K}_x\text{Fe}_{2-y}\text{S}_2$.¹⁴ $\text{KFe}_{0.85}\text{Ag}_{1.15}\text{Te}_2$ exhibits large magnetoresistance (MR = $[\rho(H) - \rho(0)]/\rho(0)$) below about 100 K where the shoulder appears. As shown in the inset (b) of Fig. 2, the negative MR is about 30% at 1.9 K for $H = 90$ kOe. This behavior is distinctively different from $\text{K}_x\text{Fe}_{2-y}\text{S}_2$, which does not show any MR in measured temperature range.¹⁴

Figure 3(a) presents the temperature dependence of magnetic susceptibility $\chi(T)$ of the $\text{KFe}_{0.85}\text{Ag}_{1.15}\text{Te}_2$ single crystal for $H = 1$ kOe along the ab plane and the c axis below 300 K with zero-field-cooling (ZFC) and field-cooling (FC). The $\chi_{ab}(T)$ is slightly larger than $\chi_c(T)$ and above 50 K, both can be fitted very well using Curie-Weiss law $\chi(T) = \chi_0 + C/(T - \theta)$, where χ_0 includes core diamagnetism, van Vleck and Pauli paramagnetism, C is Curie constant and θ is the Curie-Weiss temperature (solid lines in Fig. 3(a)). The fitted parameters are $\chi_0 = 5.46(7) \times 10^{-6}$ emu $\text{g}^{-1} \text{Oe}^{-1}$, $C = 2.58(3) \times 10^{-3}$ emu $\text{g}^{-1} \text{Oe}^{-1} \text{K}$, and $\theta = -82(1)$ K for $H \parallel ab$ and χ_0

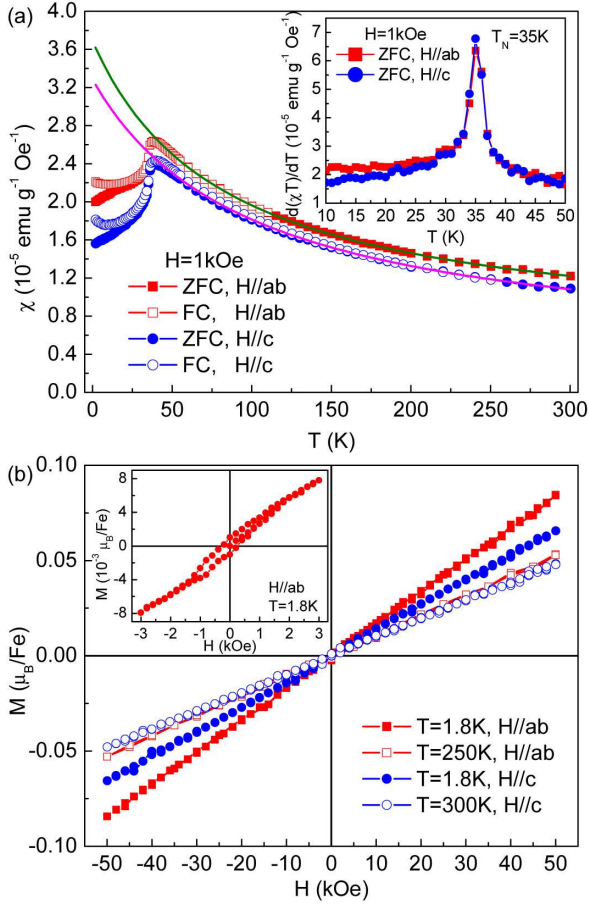


FIG. 3. (a) Temperature dependence of DC magnetic susceptibility $\chi(T)$ with the applied field $H = 1$ kOe along ab plane and c axis below 300 K under ZFC and FC mode. The inset shows $d(\chi T)/dT$ result for both field directions. (b) Isothermal magnetization hysteresis loops $M(H)$ for H//ab and H//c at various temperatures.

$= 3.5(1) \times 10^{-6}$ emu g^{-1} Oe $^{-1}$, $C = 2.92(5) \times 10^{-3}$ emu g^{-1} Oe $^{-1}$ K, and $\theta = -100(2)$ K for H//c. The above values of C correspond to an effective moment of $\mu_{eff} = 3.60(2) \mu_B/Fe$ and $3.83(3) \mu_B/Fe$ for H//ab and H//c, respectively. The values of μ_{eff} are smaller than for free Fe $^{2+}$ ions ($4.7 \mu_B/Fe$) and Fe $_{1+x}$ Te ($4.9 \mu_B/Fe$),²² but slightly larger than in K $_x$ Fe $_{2-y}$ Se $_2$ ($3.31 \mu_B/Fe$).²³

We observe sharp drops below 35 K in both ZFC and FC curves, associated with the onset of long-range AFM order. The $T_N = 35$ K is determined from the peak of $d(\chi T)/dT$ (inset of Fig. 3(a)).²⁴ It should be noted that antiferromagnetism below 35 K and Curie-Weiss paramagnetism at higher temperature are obviously different from K $_x$ Fe $_{2-y}$ Se $_2$ and K $_x$ Fe $_{2-y}$ S $_2$.¹³ Fig. 3 (b) shows the magnetization loops for both field directions at various temperatures. It can be seen that all M-H loops exhibit almost linear field dependence and $M(H)$ curve exhibits a very small hysteresis at 1.8 K with the small coercive field (~ 260 Oe).

Figure 4 shows the temperature dependence of heat capacity C_p for KFe $_{0.85}$ Ag $_{1.15}$ Te $_2$ single crystals measured

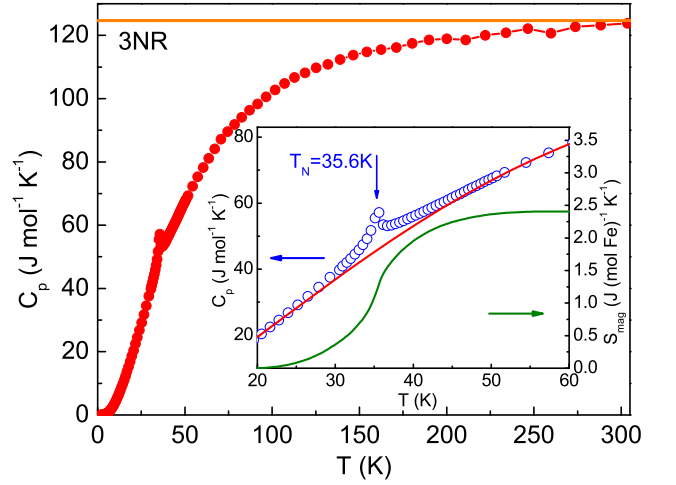


FIG. 4. Temperature dependence of heat capacity for KFe $_{0.85}$ Ag $_{1.15}$ Te $_2$ single crystal. The orange solid line represents the classical value according to Dulong-Petit law at high temperature. The inset shows the enlarged area near magnetic transition region of $C_p - T$. The red solid curve represents the lattice contribution, fitted by a polynomial. The right label denotes the magnetic entropy associated with the AFM transition.

between $T = 1.95$ and 300 K in a zero magnetic field. At high temperature heat capacity approaches the Dulong-Petit value of 3NR, where N is the atomic number in the chemical formula ($N = 5$) and R is the gas constant ($R = 8.314$ J mol $^{-1}$ K $^{-1}$). On the other hand, at the low temperature $C_p(T)$ curve can be fitted solely by a cubic term βT^3 . By neglecting antiferromagnon contribution,²⁵ from the fitted value of $\beta = 3.11(2)$ mJ mol $^{-1}$ K $^{-4}$, the Debye temperature is estimated to be $\Theta_D = 146.2(3)$ K using the formula $\Theta_D = (12\pi^4 NR/5\beta)^{1/3}$. This is much smaller than Θ_D of K $_x$ Fe $_{2-y}$ Se $_2$ and K $_x$ Fe $_{2-y}$ S $_2$ at least partially because of larger atomic mass of Ag and Te in KFe $_{0.85}$ Ag $_{1.15}$ Te $_2$.^{14,26}

A λ -type anomaly at $T_N = 35.6$ K (shown in the inset of Fig. 4) confirms the bulk nature of the AFM order observed in the magnetization measurement shown in Fig. 3. The transition temperature is consistent with the values determined from $d(\chi T)/dT$ (35 K). Assuming that the total heat capacity consists of phonon (C_{ph}) and magnetic (C_{mag}) components, the C_{mag} can be estimated by the subtraction of C_{ph} . Consequently, the magnetic entropy (S_{mag}) can be calculated using the integral $S_{mag}(T) = \int_0^T C_{mag}/T dT$. Because of the failure of Debye model at $T > \Theta_D$, we estimated the lattice specific heat by fitting a polynomial to the $C_p(T)$ curve at temperatures well away from T_N . The obtained S_{mag} is about 2.4 J (mol Fe) $^{-1}$ K $^{-1}$ up to 60 K, which is only 18% of theoretical value ($R \ln 5 = 13.4$ J (mol Fe) $^{-1}$ K $^{-1}$ for high spin state Fe $^{2+}$ ions). Note that only about 1 J (mol Fe) $^{-1}$ K $^{-1}$ is released below T_N . This discrepancy may originate from an incorrect estimation of the lattice contribution to $C_{ph}(T)$ which can lead to reduced

$S_{mag}(T)$ or a probable short-range order that may exist above the bulk three-dimensional AFM order occurring at T_N . This could also be supported by a much smaller $T_N = 35$ K compared to the Curie-Weiss temperature $\theta = -100(2)$ K for H||c.

There are two origins could induce the negative MR effect in semiconductors: the reduction in spin disorder scattering due to the alignment of moments under a field, and the reduction of the gap arising from the splitting of the up- and down-spin subbands. The existence of AFM interaction could be related to this negative MR effect. The temperature where MR effect becomes obvious is consistent with the Curie-Weiss temperature θ , which imply this MR effect could be related to the AFM interaction and due to the reduction in spin disorder scattering with field. When compared to $K_xFe_{2-y}Se_2$, substitution of Ag has an important influence on the magnetic and transport properties. It could reduce the exchange interaction between Fe atoms and thus suppress the T_N of $KFe_{0.85}Ag_{1.15}Te_2$ significantly. On the other hand, because of the near absence of vacancies in $KFeCuS_2$ and similar valence between Cu and Ag,²⁷ it is more meaningful to compare the physical properties between $KFeCuS_2$ and $KFe_{0.85}Ag_{1.15}Te_2$. The former has the larger E_a and room-temperature resistivity than the latter. This could be due to the smaller ionic sizes of Cu and S when compared to Ag and Te, which might lead

to the smaller orbital overlap increasing E_a and resistivity. Both compounds exhibit Curie-Weiss law above 50 K and the fitted Curie-Weiss temperature are also similar (176 K for $KFeCuS_2$). Moreover, $KFeCuS_2$ shows magnetic transition at 40 K, which is very close to the T_N of $KFe_{0.85}Ag_{1.15}Te_2$. However, the transition of $KFeCuS_2$ is spin glass-like, in contrast to the long-range AFM order of $KFe_{0.85}Ag_{1.15}Te_2$. This implies that the distribution of Ag in $KFe_{0.85}Ag_{1.15}Te_2$ may be different from Cu in $KFeCuS_2$ which results in different magnetic ground state configuration with similar interaction strength.

In summary, we successfully synthesized the $K_{1.00(3)}Fe_{0.85(2)}Ag_{1.15(2)}Te_{2.0(1)}$ single crystals with $ThCr_2Si_2$ structure, identical to $K_{0.8}Fe_{2-y}Se_2$ at 600 K. Crystal structure and composition analysis indicate that there are no K, Fe/Ag and Te vacancies within 3, 2, or 5 atomic %, respectively. Transport, magnetic, and thermal measurements indicate that the $KFe_{0.85}Ag_{1.15}Te_2$ is a semiconductor with long-rang AFM order below 35 K.

We thank John Warren for help with scanning electron microscopy measurements and Jonathan Hanson for help with X-ray measurements. Work at Brookhaven is supported by the U.S. DOE under Contract No. DE-AC02-98CH10886 and in part by the Center for Emergent Superconductivity, an Energy Frontier Research Center funded by the U.S. DOE, Office for Basic Energy Science

-
- ¹ Y. Kamihara, T. Watanabe, M. Hirano, and H. Hosono, *J. Am. Chem. Soc.* **130**, 3296 (2008).
- ² M. Rotter, M. Tegel, and D. Johrendt, *Phys. Rev. Lett.* **101**, 107006 (2008).
- ³ X. C. Wang, Q. Q. Liu, Y. X. Lv, W. B. Gao, L. X. Yang, R. C. Yu, F. Y. Li, and C. Q. Jin, *Solid State Commun.* **148**, 538 (2008).
- ⁴ F. C. Hsu, J. Y. Luo, K. W. Yeh, T. K. Chen, T. W. Huang, P. M. Wu, Y. C. Lee, Y. L. Huang, Y. Y. Chu, D. C. Yan, and M. K. Wu, *Proc. Natl. Acad. Sci. USA* **105**, 14262 (2008).
- ⁵ K.-W. Yeh, T. W. Huang, Y. L. Huang, T. K. Chen, F. C. Hsu, P. M. Wu, Y. C. Lee, Y. Y. Chu, C. L. Chen, J. Y. Luo, D. C. Yan, and M. K. Wu, *EPL* **84**, 37002 (2008).
- ⁶ Y. Mizuguchi, F. Tomioka, S. Tsuda, T. Yamaguchi, and Y. Takano, *Appl. Phys. Lett.* **94**, 012503 (2009).
- ⁷ J. Guo, S. Jin, G. Wang, S. Wang, K. Zhu, T. Zhou, M. He, and X. Chen, *Phys. Rev. B* **82**, 180520(R) (2010).
- ⁸ C.-H. Li, B. Shen, F. Han, X. Y. Zhu, and H.-H. Wen, *Phys. Rev. B* **83**, 184521 (2011).
- ⁹ A. Krzton-Maziopa, Z. Shermadini, E. Pomjakushina, V. Pomjakushin, M. Bendele, A. Amato, R. Khasanov, H. Luetkens, and K. Conder, *J. Phys.: Condens. Matter* **23**, 052203 (2011).
- ¹⁰ M. H. Fang, H. D. Wang, C. H. Dong, Z. J. Li, C. M. Feng, J. Chen, H. Q. Yuan, *EPL* **94**, 27009 (2011).
- ¹¹ C. de la Cruz, Q. Huang, J. W. Lynn, J. Li, W. Ratcliff, II, J. L. Zarestky, H. A. Mook, G. F. Chen, J. L. Luo, N. L. Wang, and P. Dai, *Nature* **453**, 899 (2008).
- ¹² Y. Zhang, L. X. Yang, M. Xu, Z. R. Ye, F. Chen, C. He, H. C. Xu, J. Jiang, B. P. Xie, J. J. Ying, X. F. Wang, X. H. Chen, J. P. Hu, M. Matsunami, S. Kimura, and D. L. Feng, *Nat. Mater.* **10**, 273 (2011).
- ¹³ H. C. Lei, K. F. Wang, J. B. Warren, and C. Petrovic, arXiv:1102.2434 (2011).
- ¹⁴ H. C. Lei, M. Abeykoon, E. S. Bozin, and C. Petrovic, *Phys. Rev. B* **83**, 180503(R) (2011).
- ¹⁵ I. R. Shein and A. L. Ivanovskii, *J. Supercond. Nov. Magn.* (online first) (2011).
- ¹⁶ H. C. Lei and C. Petrovic, *Phys. Rev. B* **83**, 184504 (2011).
- ¹⁷ A. C. Larson and R. B. Von Dreele, Los Alamos National Laboratory Report LAUR 86-748 (1994).
- ¹⁸ B. H. Toby, *J. Appl. Cryst.* **34**, 210 (2001).
- ¹⁹ J. Li, H.-Y. Guo, and R. A. Yglesias, *Chem. Mater.* **7**, 599 (1995).
- ²⁰ E. E. Rodriguez, P. Zavalij, P.-Y. Hsieh, and M. A. Green, *J. Am. Chem. Soc.* **132**, 10006 (2010).
- ²¹ D. M. Wang, J. B. He, T.-L. Xia, and G. F. Chen, *Phys. Rev. B* **83**, 132502 (2011).
- ²² Y. Liu, R. K. Kremer, and C. T. Lin, *Supercond. Sci. Technol.* **24**, 035012 (2011).
- ²³ W. Bao, Q. Huang, G. F. Chen, M. A. Green, D. M. Wang, J. B. He, X. Q. Wang, and Y. Qiu, arXiv:1102.0830 (2011).
- ²⁴ M. E. Fisher, *Philos. Mag.* **7**, 1731 (1962).
- ²⁵ J. van Kranendonk and J. H. van Vleck, *Rev. Mod. Phys.* **30**, 1 (1958).
- ²⁶ B. Zeng, B. Shen, G. F. Chen, J. B. He, D. M. Wang, C. H. Li, and H. H. Wen, *Phys. Rev. B* **83**, 144511 (2011).
- ²⁷ M. Oledzka, K. V. Ramanujachary, and M. Greenblatt, *Mater. Res. Bull.* **31**, 1491 (1996).